The metabolic response of *Pseudomonas taiwanensis* to NADH dehydrogenase deficiency

Salome C. Nies[1], Robert Dinger[2], Yan Chen[3], Gossa G. Wordofa[4], Mette Kristensen[4], Konstantin Schneider[4], Jochen Büchs[2], Christopher J. Petzold[3,5], Jay D. Keasling[3,4,5,6,7,8], Lars M. Blank[1*], Birgitta E. Ebert[1§]

[1]iAMB-Institute of Applied Microbiology, ABBt-Aachen Biology and Biotechnology, RWTH Aachen University, DE
[2]AVT – Biochemical Engineering, RWTH Aachen University, DE
[3]Joint BioEnergy Institute, Emeryville, CA 94608, USA.
[4]Novo Nordisk Foundation Center for Biosustainability, Technical University of Denmark, DK-2800 Lyngby, DK
[5]Lawrence Berkeley National Laboratory, Biological Systems and Engineering Division, Berkeley, CA 94720, USA.
[6]Virtual Institute of Microbial Stress and Survival, Lawrence Berkeley National Laboratory, Berkeley, CA
[7]Physical Biosciences Division, Lawrence Berkeley National Laboratory, Berkeley, CA
[8]Dept. of Bioengineering, University of California, Berkeley, CA
[9]Dept. of Chemical Engineering, University of California, Berkeley, CA
[10]Synthetic Biochemistry Center, Institute for Synthetic Biology, Shenzhen Institutes for Advanced Technologies, Shenzhen, China

* Corresponding author
§ Present address: Australian Institute for Bioengineering and Nanotechnology (AIBN), The University of Queensland, Brisbane, QLD 4072, Australia

Running title: NADH dehydrogenase deficiency in *P. taiwanensis*

Keywords *Pseudomonas*; NADH dehydrogenase; respiratory activity; oxidative stress; electron transport chain

Abstract

Obligate aerobic organisms rely on a functional electron transport chain for energy generation and NADH oxidation. Because of this essential requirement, the genes of this pathway are likely constitutively and highly expressed to avoid a cofactor imbalance and energy shortage under fluctuating environmental conditions.

We here investigated the essentiality of the three NADH dehydrogenases of the respiratory chain of the obligate aerobe *Pseudomonas taiwanensis* VLB120 and the impact of the knockouts of corresponding genes on its physiology and metabolism. While a mutant lacking all three NADH dehydrogenases seemed to be nonviable, the generated single or double knockout strains displayed none or only a marginal phenotype. Only the mutant deficient in both type 2 dehydrogenases showed a clear phenotype with biphasic growth behavior and strongly reduced growth rate in the second phase. In-depth analyses of the metabolism of the generated mutants including quantitative physiological experiments, transcript analysis, proteomics and enzyme activity assays revealed distinct responses to type II and type I dehydrogenase deletions. An overall high metabolic flexibility enables *P. taiwanensis* to cope with the introduced genetic perturbations and maintain stable phenotypes by rerouting of metabolic fluxes.

This metabolic adaptability has implications for biotechnological applications. While the phenotypic robustness is favorable in large-scale applications with inhomogeneous conditions, versatile redirecting of carbon fluxes upon genetic interventions can frustrate metabolic engineering efforts.

Importance

While *Pseudomonas* has the capability for high metabolic activity and the provision of reduced redox cofactors important for biocatalytic applications, exploitation of this

characteristic might be hindered by high, constitutive activity of and consequently competition with the NADH dehydrogenases of the respiratory chain. The in-depth analysis of NADH dehydrogenase mutants of *Pseudomonas taiwanensis* VLB120 presented here, provides insight into the phenotypic and metabolic response of this strain to these redox metabolism perturbations. The observed great metabolic flexibility needs to be taken into account for rational engineering of this promising biotechnological workhorse towards a host with controlled and efficient supply of redox cofactors for product synthesis.

Introduction

Many industrially relevant molecules, e. g., ethanol, butanediol or isoprene, are more reduced than the industrially-used sugars glucose and sucrose or alternative, upcoming carbon sources such as xylose or glycerol (1-3). The microbial production of those favored compounds hence is inherently redox limited, i.e. by the supply of reduced redox cofactors, generally NADH or NADPH. This bottleneck has been overcome in some cases, e.g., 1,4 butanediol and 1,3-propanediol production in *Escherichia coli* (4, 5) or L-lysine synthesis in *Corynebacterium glutamicum* (6). Applied strategies are optimization of the host metabolism by metabolic engineering (4, 7, 8) or adaptation of process conditions by (co-)feeding reduced substrates (9), applying microaerobic conditions or by nongrowing cells with reduced competition and cellular demand for the redox cofactor (10-13). Alternatively, microorganisms can be applied that naturally outperform the classic, industrial workhorses with respect to redox cofactor supply. Pseudomonads are outstanding in this regard as they exhibit a driven-by-demand phenotype, which allows them to strongly enforce the metabolic activity under stress conditions with increased energy demand, reported to result in a more than 2-fold carbon uptake rate and an even 8-fold increase of the NAD(P)H regeneration rate relative to standard growth conditions (12, 14, 15). This behavior holds great promise for using this species for the bioproductions of highly reduced chemicals such as phenol, (*S*)-styrene oxide, rhamnolipids, and methyl ketones (16-20). Yet, competition is high as the NAD^+/NADH couple functions as cofactor in over 300 oxidation/reduction reactions (21). The obligate aerobic lifestyle of *Pseudomonas* without apparent fermentative metabolism necessitates constitutive activity of the NADH dehydrogenases to ensure adequate oxidation of NADH to NAD^+. Hence, we argue here that a naturally high NADH oxidation activity might impair the effective fueling of production pathways with reducing equivalents. We here set out to provide an in-depth analysis of the redox metabolism of *Pseudomonas taiwanensis* VLB120, a strictly aerobic bacterium, focusing

on the role and essentiality of the single NADH dehydrogenases for NADH oxidation and energy generation.

The genome of *P. taiwanensis* VLB120 encodes two types of NADH dehydrogenases, type I (EC 7.1.1.2) and two isoforms of type II (EC 1.6.99.3). Type I is encoded by the genes PVLB_15600-15660 designated as the *nuo* operon and often referred to as complex 1 (22). Nuo is a multisubunit enzyme complex and couples the electron transfer to proton translocation (23). The resulting proton gradient can then be used by the ATP synthase for the generation of ATP. The two type II NADH dehydrogenases, also termed alternative NADH dehydrogenase, are encoded by PVLB_13270 and PVLB_21880, designated as *ndh1* and *ndh2*, respectively. Ndh1 and Ndh2, both consist of a single polypeptide chain; they transfer electrons from NADH to ubiquinone but do not contribute to the membrane potential (23, 24). The amino acid sequence of the NADH dehydrogenases *ndh2* and *nuoA-N* of *P. taiwanensis* VLB120 and *Pseudomonas putida* KT2440 share a 96% homology.

In this study, NADH dehydrogenase mutants of *P. taiwanensis* VLB120 were generated and characterized regarding growth, respiratory activity, and transcriptional and proteomic changes to elucidate the impact of redox metabolism perturbation on the cellular physiology.

Materials and Methods

Strains, media and culture conditions

Bacterial strains used in this study are listed in Table 1. Strains were propagated in Lysogeny Broth (LB) containing 10 g L^{-1} peptone, 5 g L^{-1} sodium chloride, and 5 g L^{-1} yeast extract (25). Cetrimide agar (Sigma-Aldrich, St. Louis, MO, USA) was used after mating procedures to select for *Pseudomonas*. Growth and characterization experiments were performed using mineral salt medium (MSM) (26) containing 3.88 g L^{-1} K_2HPO_4, 1.63 g L^{-1} NaH_2PO_4, 2 g L^{-1} $(NH_4)_2SO_4$, 0.1 g L^{-1} $MgCl_2 \cdot 6H_2O$, 10 mg L^{-1}

EDTA, 2 mg L^{-1} $ZnSO_4 \cdot 7\ H_2O$, 1 mg L^{-1} $CaCl_2 \cdot 2H_2O$, 5 mg L^{-1} $FeSO_4 \cdot 7\ H_2O$, 0.2 mg L^{-1} $Na_2MoO_4 \cdot 2H_2O$, 0.2 mg L^{-1} $CuSO_4 \cdot 5\ H_2O$, 0.4 mg L^{-1} $CoCl_2 \cdot 6\ H_2O$, 1 mg L^{-1} $MnCl_2 \cdot 2\ H_2O$ supplemented with 25 mM glucose. For preparation of solid LB, 1.5% agar was added to the medium. For plasmid maintenance and in the gene deletion procedure, antibiotics were added to the medium as required. Gentamycin and Kanamycin were used at concentrations of 25 mg L^{-1} and 50 mg L^{-1}, respectively.

Table 1 Bacterial strains used in this study.

Strain	Relevant characteristics[a]	Reference
E. coli		
DH5α	*fhuA*2 *lac*(del)U169 *phoA glnV*44 Φ80' *lacZ*(del)M15 *gyrA*96 *recA*1 *relA*1 *endA*1 *thi*-1 *hsdR*17	NEB
DH5αλpir1	F−, Δlac169, rpoS(Am), robA1, creC510, hsdR514, endA, recA1uidA(ΔMluI)::pir-116; host for oriV(R6K) vectors in high copy number	Thermo Fisher Scientific
HB101 pRK2013	SmR, hsdR-M+, proA2, leuB6, thi-1, recA; bears plasmid pRK2013	(27)
DH5α pSW-2	Gm^r, DH5α bearing pSW-2	(28)
DH5αλpir1 pEMG	Km^r, DH5αλpir1 bearing plasmid pEMG	(28)
DH5αλpir1 pEMG_ko_ndh1	Km^r, PVLB_13270 deletion plasmid	This study
DH5αλpir1 pEMG_ko_ndh2	Km^r, PVLB_21880 deletion plasmid	This study
DH5αλpir1 pEMG_ko_nuo	Km^r, PVLB_15600-15660 deletion plasmid	This study
P. taiwanensis		
VLB120	wild type	(29)
VLB120 $pSTY^-$	VLB120 devoid of megaplasmid pSTY	Wynands et al. submitted
VLB120 Δ*ndh1*	Δ*ndh1* (PVLB_13270), $pSTY^-$	This study
VLB120 Δ*ndh2*	Δ*ndh2* (PVLB_21880), $pSTY^-$	This study
VLB120 ΔΔ*ndh*	ΔΔ*ndh* (PVLB_13270, PVLB_21880), $pSTY^-$	This study
VLB120 Δ*nuo*	Δ*nuo* (PVLB_15600-15660), $pSTY^-$	This study
VLB120 Δ*nuo*Δ*ndh1*	Δ*ndh1* (PVLB_13270), Δ*nuo* (PVLB_15600-15660), $pSTY^-$	This study

[a] Gm^r, Km^r, gentamycin, kanamycin resistance, respectively.

Batch flask experiments were performed in 50 mL medium in 500-mL flasks on a horizontal rotary shaker with a throw of 50 mm and frequency of 300 rpm. *E. coli* was grown at 37 °C, *Pseudomonas* at 30 °C. The chemicals used in this work were obtained from Carl Roth (Karlsruhe, Germany), Sigma-Aldrich (St. Louis, MO, USA), or Merck (Darmstadt, Germany), unless stated otherwise. The main cultures were inoculated from liquid pre-cultures to an approximate OD_{600nm} of 0.05. All experiments were performed in biological triplicates unless stated otherwise.

Plasmid cloning and generation of deletion strains

Genomic DNA of *P. taiwanensis* VLB120 was isolated using the High Pure PCR Template Preparation Kit (Hoffmann-La-Roche, Basel, Switzerland). Upstream (TS1) and downstream (TS2) regions with a length of 400-800 bp flanking the specific target gene were amplified using Q5 High-Fidelity Polymerase (New England Biolabs, Ipswich, MA, USA). Primers were ordered as unmodified DNA Oligonucleotides from Eurofins Genomics (Ebersberg, Germany) and are listed in Supplementary Table S1. The suicide delivery vector pEMG was isolated using the NEB Monarch Plasmid Miniprep Kit (New England Biolabs, Ipswich, MA, USA). The isolated plasmid was digested with restriction enzymes purchased from New England Biolabs (Ipswich, MA, USA). For plasmid construction, Gibson Assembly using NEB Builder Hifi DNA Assembly (New England Biolabs, Ipswich, MA, USA) was used. Plasmids were transformed into electrocompetent *E. coli* DH5αλpir1 via electroporation (30). Transformants and chromosomally engineered *Pseudomonas* were screened by colony PCR using OneTaq 2x Master Mix (New England Biolabs, Ipswich, MA, USA). The cell material was lysed in alkaline polyethylene glycol for enhanced colony PCR efficiency as described previously (31).

Targeted gene deletions were performed using the I-SceI-based system developed by Martinez-Garcia and de Lorenzo (28). The conjugational transfer of the mobilizable

knock-out plasmids from *E. coli* DH5αλpir1 to *Pseudomonas* was performed via triparental patch mating (16). After conjugation, the pSW-2 plasmid encoding the I-SceI-endonuclease was conjugated into *Pseudomonas* co-integrates. The addition of 3-methylbenzoate for the induction of I-SceI expression was omitted as the basal expression level was sufficient. Kanamycin-selective clones were directly isolated, positive clones were cured of pSW-2 and restreaked several times. The gene deletion was confirmed by colony PCR and Sanger sequencing.

Analytical methods

The optical density of cell suspensions was measured at a wavelength of 600 nm using an Ultrospec 10 spectrophotometer (GE Healthcare, Chicago, IL, USA). The cell dry weight (CDW) was calculated by multiplying OD_{600nm} with a gravimetrically determined correlation factor of 0.39. For HPLC analysis the samples were centrifuged at 17,000 x g for 5 min and the supernatant was stored at -20°C until further analysis.

Glucose and gluconate concentrations were measured by high-performance liquid chromatography using a Beckman System Gold 126 Solvent Module equipped with a System Gold 166 UV-detector (Beckman Coulter) and a Smartline RI detector 2300 (KNAUER Wissenschaftliche Geräte, Berlin, Germany). Analytes were separated on the organic resin column Metab AAC (ISERA, Düren, Germany) eluted with 5 mM H_2SO_4 at an isocratic flow of 0.6 mL min^{-1} at 40 °C for 20 min. Glucose and gluconate were analyzed using the RI detector whereas gluconate was determined with the UV detector at a wavelength of 210 nm.

Proteomic profiling of NADH dehydrogenase mutants

Samples for proteome profiling were taken during early-, mid-, and late-exponential growth at an OD_{600nm} of 0.5, 2.5, and after depletion of glucose, checked with test strips for rapid detection of glucose (Medi-Test, Macherey-Nagel, Düren, Germany), respectively. Proteins were extracted from cell biomass and subsequently prepared for shotgun proteomic experiments as described previously (32). All samples were

analyzed on an Agilent 6550 iFunnel Q-TOF mass spectrometer (Agilent Technologies, Santa Clara, CA) coupled to an Agilent 1290 UHPLC system. Twenty (20) µg of peptides were separated on a Sigma–Aldrich Ascentis Peptides ES-C18 column (2.1 mm × 100 mm, 2.7 µm particle size, operated at 60°C) at a 0.400 mL min^{-1} flow rate and eluted with the following gradient: initial condition was 95% solvent A (0.1% formic acid) and 5% solvent B (99.9% acetonitrile, 0.1% formic acid). Solvent B was increased to 35% over 120 min, and then increased to 50% over 5 min, then up to 90% over 1 min, and held for 7 min at a flow rate of 0.6 mL min^{-1}, followed by a ramp back down to 5% B over 1 min where it was held for 6 min to re-equilibrate the column to original conditions. Peptides were introduced to the mass spectrometer from the LC by using a Jet Stream source (Agilent Technologies) operating in positive-ion mode (3,500 V). Source parameters employed gas temp (250°C), drying gas (14 L min^{-1}), nebulizer (35 psig), sheath gas temp (250°C), sheath gas flow (11 L min^{-1}), VCap (3,500 V), fragmentor (180 V), OCT 1 RF Vpp (750 V). The data were acquired with Agilent MassHunter Workstation Software, LC/MS Data Acquisition B.06.01 operating in Auto MS/MS mode whereby the 20 most intense ions (charge states, 2–5) within 300–1,400 m/z mass range above a threshold of 1,500 counts were selected for MS/MS analysis. MS/MS spectra (100–1,700 m/z) were collected with the quadrupole set to “medium” resolution and were acquired until 45,000 total counts were collected or for a maximum accumulation time of 333 ms. Former parent ions were excluded for 0.1 min following MS/MS acquisition. The acquired data were exported as mgf files and searched against the pan proteome that is highly related to *Pseudomonas taiwanensis* VLB120 with Mascot search engine version 2.3.02 (Matrix Science). The resulting search results were filtered and analyzed by Scaffold v 4.3.0 (Proteome Software Inc.). The normalized spectra count of each sample were exported from Scaffold, and the relative quantity changes of identified proteins in mutant samples were calculated in comparison to wild type sample. The statistical significance of these changes and the adjusted p-

values were evaluated by limma R package. The mass spectrometry proteomics data have been deposited to the ProteomeXchange Consortium via the PRIDE (33) partner repository with the dataset identifier PXD013623 and 10.6019/PXD013623.

RNA preparation and analysis

Samples for transcription analysis were taken during early-, mid- and late-exponential growth at an OD_{600nm} of approximately 0.5, approximately 2.5 and after glucose depletion, respectively. Prior to RNA isolation, the culture sample was diluted with the DNA/RNA protection reagent of the Monarch Total RNA Miniprep Kit (New England Biolabs, Ipswich, MA, USA), followed mechanical lysis with ZR BashingBead™ Lysis Tube (0.5mm) (Zymo Research, Irvine, CA, USA) for 1 min using the Mini-Beadbeater-16 (Biospec, Bartlesville, OK, USA). After a centrifugation step at 16,000 x g for 2 min the supernatant was transferred into a new tube. An equal volume of RNA lysis buffer of the Monarch Total RNA Miniprep Kit was added, and the RNA isolation was continued as described in the supplier's manual. After the last elution step, an additional in-tube DNase treatment was done using RNase-free DNaseI (New England Biolabs, Ipswich, MA, USA). The final RNA yield and purity were evaluated by the absorption ratio A_{260}/A_{280} measured with a Nanodrop (Thermo Scientific, Rockford, IL, USA). The synthesis of cDNA for reverse transcription was carried out with a Protoscript II first strand cDNA synthesis kit (New England Biolabs, Ipswich, MA, USA) using 120 ng total RNA and 60 µM random hexamers. The qPCR analyses were conducted with 5 µL of the reverse transcription reaction mixture with gene-specific primers (Supplementary Table S1) and the Luna Universal qPCR Master Mix (New England Biolabs, Ipswich, MA, USA) was used. Primers for qPCR were designed with the PrimerQuest Tool of IDT technologies. Gene expression levels for each individual sample were normalized relative to the internal reference gene, *rpoB* and the wild type in the corresponding growth phase calculated by a mathematical method based on the calculated real-time PCR efficiencies (34). The qPCR was performed with the CFX96 Real-Time PCR

Detection System (Biorad, Hercules, CA, USA). All qPCR reactions were performed in triplicates.

Inverted membrane vesicle preparation and NADH oxidation activity

Cultures were harvested at early-exponential growth phase at an optical density (OD_{600nm}) of approximately 0.5, as well as in the late-exponential growth phase ($OD_{600nm,}$ of 3-4). Inverted membrane vesicles were prepared as described by Borisov (35). Briefly, cells were centrifuged for 8 min at 5,000 x g and resuspended in 2 mL spheroblast buffer (200 mM Tris-HCl pH 8.0, 2 mM EDTA, 30% sucrose), centrifuged again and resuspended in 1 mL spheroplast buffer. Spheroplasts were prepared using lysozym (0.03 g) and incubated for 30 min at room temperature. Spheroplasts were centrifuged for 10 min at 5,000 x g and resuspended in 2 mL sonication buffer (100 mM HEPES-KOH pH 7.5, 50 mM K_2SO_4, 10 mM $MgSO_4$, 2 mM DTT, 0.5 mM PMSF). The vesicles were sonicated (Bioruptor, Diadenode, Belgium) in 4 cycles à 30 sec at high intensity with an intermediate pause of 30 sec in ice water. The inverted membrane vesicles were centrifuged twice for 10 min at 5,000 x g to remove cell debris. The supernatant was centrifuged for 30 min at 120,000 x g and the resulting pellet was resuspended in the assay buffer (25 mM HEPES, 25 mM BIS-TRIS propane pH 7, 10 mM $MgSO_4$).

The freshly prepared inverted membrane vesicles were immediately used for the determination of the NADH oxidation activity as we observed a rapid activity decline when the membrane samples were stored on ice. 150 µL mL^{-1} isolated membrane fractions were added to the assay buffer and the reaction was initiated by the addition of 125 µM NADH, the total volume of the assay was 200 µL. The NADH oxidation was monitored over 30 min at 340 nm in a Synergy^{TM} MX microplate reader (BioTek, Winooski, VT, USA). For calculating the specific enzyme activity, we used the NADH molar extinction coefficient ε_{NADH} = 6.22 mM^{-1} cm^{-1}; one unit of activity was the quantity that catalyzed the oxidation of 1 µmol of NADH per min. The protein concentration was

measured with the reducing agent compatible Pierce BCA Protein Assay Kit (Thermo Scientific, Rockford, IL, USA).

Respiration activity monitoring

The cultivations and measurements of the oxygen transfer rate (OTR) and the carbon dioxide transfer rate (CTR) were performed in a modified RAMOS System, developed by the Chair of Biochemical Engineering (RWTH Aachen University) (36, 37). The standard RAMOS for shake flasks is commercially available from the Kühner AG (Birsfelden, Switzerland) or HiTec Zang GmbH (Herzogenrath, Germany). All cultivations were performed in 250-mL Ramos flasks with 10 % (v/v) filling volume using MSM medium supplemented with 25 mM glucose. The cultures were inoculated from liquid pre-cultures to an approximate OD_{600nm} of 0.05. The OTR and CTR were measured thrice per hour. All experiments were performed in biological duplicates.

Redox cofactor quantification

Samples for redox cofactor analysis were collected from early-, mid-, and late-exponential growth phase at OD_{600nm} of approximately 0.6, 2.2 and 4.0, respectively. The samples were rapidly transferred into a 15-mL falcons tube containing 5 mL of quenching solution (acetonitrile:methanol:water, 40:40:20, v/v) with ^{13}C labelled cell extracts at –40℃.

After three freeze-thaw cycles, the samples were centrifuged at 13,000 x g for 5 min and concentrated by evaporating the quenching solvent using a vacuum concentrator (SAVANT, SpeedVac, Thermo Fisher Scientific, San Diego, CA, USA) for 5 hours followed by lyophilization (LABCONCO, FreeZone, Kansas City, MO, USA). All dried extracts were stored −80°C until analysis or re-suspended in LC-MS grade water for LC-MS analysis.

All redox cofactor metabolites were measured on an AB SCIEX Qtrap1 5500 mass spectrometer (AB SCIEX, Framingham, MA, USA) operated in negative ion and

287 selected multiple reaction monitoring (MRM) mode. The column XSELECT HSS XP
288 (150 mm × 2.1 mm × 2.5 µm) (Waters, Milford, MA, USA) with ion-pairing technique was
289 used for the chromatography separation as previously described (38). Peak integration
290 and metabolite quantification were performed using an isotope-ratio-based approach on
291 Multi-QuantTM 3.0.2 (AB SCIEX) software as previously described (39, 40).

Results

P. taiwanensis VLB120 can easily compensate for single NADH dehydrogenase gene deletions.

The NADH dehydrogenase type I operon encoded by *nuoA-N* (PVLB_15600-15660) and the two type II NADH dehydrogenases encoded by *ndh1* (PVLB_13270) and *ndh2* (PVLB_21880) were successfully deleted from the *P. taiwanensis* VLB120 genome using the I-SceI-based pEMG plasmid (28). The double knockout mutants ΔΔ*ndh* and Δ*nuo*Δ*ndh1* were successfully obtained, however several attempts failed to generate the double knockout of *Δnuo* and *Δndh2* (Table 2). All gene deletions were confirmed by Sanger sequencing. The five NADH-dehydrogenase mutants demonstrated that the NADH dehydrogenases, Nuo, Ndh1, and Ndh2 are not essential individually. While the presence of either Nuo or Ndh2 is sufficient to sustain viability of *P. taiwanensis* VLB120, Ndh1 seems to be unable to compensate for the loss of Nuo and Ndh2. Similarly, for *P. aeruginosa* PAO1 it has been reported that single deletions of NADH dehydrogenases result in no growth defect and no decrease in NADH oxidation activity, whereas the double (Δ*nuoIJ*Δ*ndh*) and triple knockout (Δ*nuoIJ*Δ*ndh*Δ*nqrA-F*) had no NADH oxidation activity (41). Concludingly, Nuo and Ndh account for the total NADH dehydrogenase activity in this *Pseudomonas* strain. A likewise total loss of NADH dehydrogenase activity in the obligate aerobic *P. taiwanensis* VLB120 strain seems to be lethal indicating that the strain relies on the presence of NADH dehydrogenases for NADH oxidation and that alternative, native NADH consuming reactions do not suffice to efficiently re-oxidize this vital cofactor under the tested conditions.

315 **Table 2.** Overview of the NADH dehydrogenase mutants generated in this study. 'X
316 'indicates successful gene deletion.

Strain	NADH dehydrogenase type I	NADH dehydrogenase type II	
	***nuoA-N* (PVLB_15600-15660)**	***ndh1* (PVLB_13270)**	***ndh2* (PVLB_21880)**
Wild type	present	present	present
Δ*ndh1*[a]	present	X	present
Δ*ndh2*[a]	present	present	X
ΔΔ*ndh*[a]	present	X	X
Δ*nuo*[a]	X	present	present
Δ*nuo*Δ*ndh1*[a]	X	X	present

317 [a] The megaplasmid pSTY (42) was absent in all mutants.

318

319 **The ΔΔ*ndh* mutant showed a growth-phase dependent growth defect**

320 *P. taiwanensis* VLB120 and the five NADH dehydrogenase deletion strains Δ*ndh1*,
321 Δ*ndh2*, ΔΔ*ndh*, Δ*nuo*, and Δ*nuo*Δ*ndh1* were characterized for growth, glucose utilization,
322 CO_2 formation, and oxygen consumption in batch shake-flask experiments. The single
323 NADH-dehydrogenase type II mutants, Δ*ndh1* and Δ*ndh2*, showed the same growth and
324 sugar co-utilization profile as the wild type *P. taiwanensis* VLB120 (Figure 1A, B, and
325 C). The loss of the megaplasmid pSTY during NADH dehydrogenase deletions resulted
326 in a growth advantage for the generated mutants, which was determined to result in a
327 14% higher growth rate for *P. taiwanensis* VLB120 $pSTY^-$ compared to the $pSTY^+$ wild
328 type (data not shown). For a comparison of mutants and wild type, the growth rate of
329 the wild type was corrected accordingly and is referred to as μ_{recalc}.
330 Both NADH dehydrogenases type I mutants Δ*nuo* and Δ*nuo*Δ*ndh1* exhibited wild type-
331 like growth and carbon uptake rates (Figure 1, Table 3). However, the glucose utilization
332 in both type 1 deletion strains differed remarkably. *Pseudomonas* can catabolize
333 glucose either via the phosphorylative or the oxidative pathway. In the latter, glucose is
334 oxidized to gluconate in the periplasm by a membrane-bound glucose dehydrogenase
335 (*gcd*) coupled to the reduction of pyrroloquinoline quinone (PQQ) (Figure 6). The
336 phosphorylative pathway starts in the cytoplasm with the phosphorylation of glucose to

337 glucose-6-phosphate catalysed by the glucokinase (Glk) (43, 44). The type I
338 dehydrogenase mutants, Δ*nuo* and Δ*nuo*Δ*ndh1*, accumulated gluconate to up to 16 mM,
339 twice as high as the concentration of the wild type and all type II deletion strains, Δ*ndh1,*
340 Δ*ndh2*, and ΔΔ*ndh* (Figure 1E-F).
341 In contrast, the type II double mutant ΔΔ*ndh* reproducibly showed two growth phases
342 (Figure 1D). After comparable growth to the wild type (Figure 1A), in the mid-
343 exponential growth phase, the growth rate dropped drastically marking the second
344 growth phase. Interestingly, the strong decrease of the growth rate (~86%) was not
345 correlated with an equal reduction of the carbon uptake, which showed a decrease of
346 only ~38%.
347

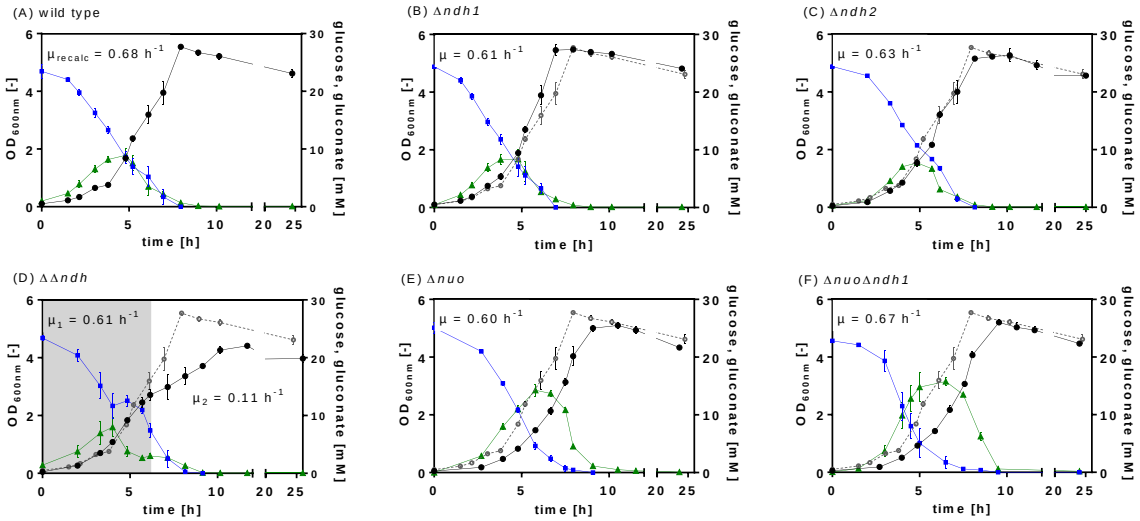

348

349 **Figure 1.** Physiological characterization of *P. taiwanensis* VLB120 (A) and the NADH
350 dehydrogenase deficient mutants Δ*ndh1* (B), Δ*ndh2* (C), ΔΔ*ndh* (D), Δ*nuo* (E), and
351 Δ*nuo*Δ*ndh1* (F). The strains were cultured in MSM with 25 mM glucose. The OD_{600nm}
352 (black circles), glucose (blue squares), gluconate (green triangles) were measured over
353 time. The shadowed area in (D) indicates the first growth phase. The data shown are
354 the mean of biological triplicates; error bars show the standard deviation. μ_{recalc} is the

growth rate of *P. taiwanensis* VLB120 pSTY$^-$. The wild type OD_{600nm} are plotted (grey, open circles) in graphs (B)-(F) for comparison.

Table 3. Calculated carbon uptake rates and gluconate and oxygen consumption of wild type and NADH dehydrogenase mutants during early-exponential growth.

Strain	Specific carbon uptake rate[a] [mmol g_{cdw}^{-1} h^{-1}]	Gluconate accumulation [mM][b]	Surplus O_2 consumption [mM][c]
wild type	7.7	8.9 ± 0.9	9.2 ± 0.9
Δ*ndh1*	6.9	8.6 ± 0.9	8.1 ± 0.1
Δ*ndh2*	7.3	7.7 ± 0.2	6.3 ± 0.4
ΔΔ*ndh*	8.8/3.3	8.8 ± 0.4	7.2 ± 1.2
Δ*nuo*	7.1	16.4 ± 0.4	12.9 ± 0.1
Δ*nuo*Δ*ndh1*	6.6	16.1 ± 1.0	14.1 ± 2.9

[a]For ΔΔ*ndh*, separate growth rates were determined for phase 1 (2-6 h) and phase 2 (6-8 h). For all other mutants, growth rates were calculated for the exponential phase (~3-4 h until ~6-7 h after inoculation); [b]gluconate accumulation was calculated from offline analytic of three biologically independent experiments; [c]the surplus oxygen consumption was calculated from the sectional integrals between the OTR (mmol L^{-1} h^{-1}) and CTR (mmol L^{-1} h^{-1}) of the first 6 hours of cultivation (Figure 2); shown is the mean of duplicate experiments.

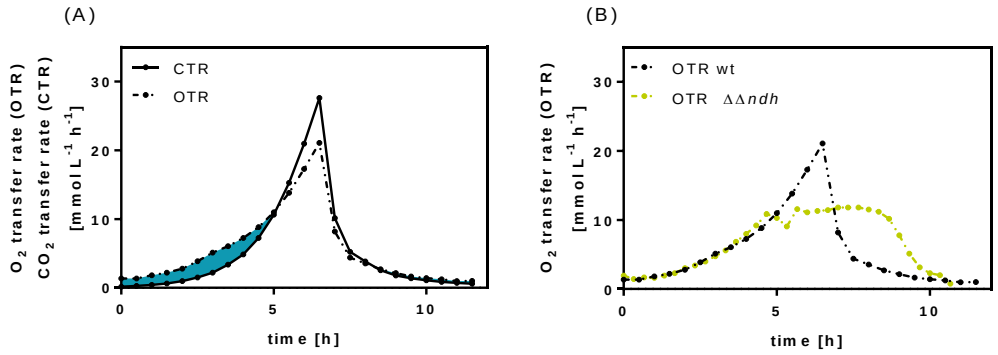

Figure 2. Respiratory activity during a cultivation of *P. taiwanensis* VLB120 and ΔΔ*ndh* mutant. (A) Highlighted area corresponding to the surplus of consumed oxygen, calculated from the sectional integrals between the OTR (dashed line, in mmol L^{-1} h^{-1}) and CTR (in mmol L^{-1} h^{-1}) on the example of *P. taiwanensis* VLB120**.** B) Oxygen transfer rates (OTR, dashed line; in mmol L^{-1} h^{-1}) during a cultivation of *P. taiwanensis* VLB120 and mutant ΔΔ*ndh.*

Besides the characterization for growth and glucose consumption, the respiratory behavior of the wild type and NADH dehydrogenase mutants was studied (Figure 2, Supplementary Figure S1). Again, only the ΔΔ*ndh* mutant showed a different phenotype characterized by a stagnating oxygen transfer rate (OTR) after 6 hours (Figure 2B). This change in the OTR development is an indication for product inhibition, here, potentially by NADH, which cannot be oxidized at the rate required for fast growth. The onset of the reduced specific oxygen uptake rate also correlated well with the change of the growth rate (Figure 1D). In case of growth on glucose, the expected respiratory quotient (RQ), defined as the ratio of OTR and CTR is close to 1. In contrast to this assumption, the measured OTR for all tested mutants during the first 6 hours of cultivation was higher than the CTR resulting in an RQ below 1 (Figure 2A, Supplementary Figure S1) due to the partial oxidation of glucose to gluconate in the periplasm (Figure 6). Indeed, the surplus of consumed oxygen calculated from the sectional integrals between the OTR and CTR ($\int OTR\,dt - \int CTR\,dt$), correlated with the produced gluconate (Table 3, Figure 2A). During glucose conversion, roughly half of the overall consumed oxygen was used for the oxidation of glucose to gluconate and the re-oxidation of the reduced PQQ formed by the glucose dehydrogenase activity. Consequently, in the glucose phase, the cells can partially uncouple glucose oxidation and energy provision from NADH formation, relieving the dependence on NADH dehydrogenase activity. The O_2 and CO_2 transfer rate (CTR) of Δ*ndh2* and ΔΔ*ndh* (Supplementary Figure S1) showed a double peak, which occurred in the same time frame as glucose depletion, and, hence, might be due to the diauxic shift from glucose to gluconate. We assume that the diauxic shift also occurred in the other strains but was not recorded by the measurement frequency of three measurements per hour.

NADH dehydrogenase gene deletions affect expression levels but do not result in altered *in vitro* NADH oxidation activities

To further elucidate the NADH oxidation activity in the different mutants, and hence, the importance of the three NADH dehydrogenases for oxidizing NADH and fueling the electron transport chain, we performed *in vitro* NADH oxidation assays. Inverted membrane vesicles were prepared at early-, mid-, and late-exponential growth phase and the NADH oxidation rate was determined from the decrease of the absorbance at 340 nm over time. As the SDS PAGE showed up to 21 prominent protein bands in the membrane fraction (data not shown), we cannot exclude activity of other membrane-bound NADH-dependent enzymes in the analyzed cytoplasmic fraction, e.g., the transhydrogenase PntAB, which might have contributed to NADH consumption. However, there is a high probability that NADH oxidation is very specific for NADH dehydrogenases as other NADH-dependent enzymes require electron acceptors other than O_2. In the early-exponential growth phase, in which none of the strains showed a growth defect, all single mutants possessed NADH oxidation activities at levels similar to the wild type of around 1.2 U mg protein^{-1} (Table 4), which is in the range of *in vitro* rates reported for other organisms (45). Overall, the NADH oxidation rate was rather stable in all mutants, indicating a high metabolic flexibility of *P. taiwanensis* VLB120 to maintain redox homeostasis.

To further substantiate this hypothesis, we examined potential changes at the transcriptional level by qPCR on samples taken in the early, mid-, and late-exponential growth phase. HPLC analysis showed that glucose and/or gluconate were still left when sampling the late-exponential growth phase, i.e., the cells were still metabolically active (data not shown). The fold changes were normalized against the wild type in the corresponding growth phase. The single and double deletions of NADH dehydrogenases type II encoding genes (Figure 3A-C) had only minor effects (max. fold change of 1) on the remaining NADH dehydrogenase gene expression. While the type I deletions strains, Δ*nuo* and Δ*nuo*Δ*ndh1*, showed a substantial upregulation of the *ndh2* gene expression (Figure 3D-E), the expression of the *ndh1* gene in both the Δ*nuo* and

429 Δ*nuo*Δ*ndh1* was unaffected; we only observed a small increase for mutant Δ*nuo* in the
430 early growth phase. This finding suggests that *ndh2* is probably the only NADH
431 dehydrogenase gene that is regulated by the cellular NADH economy. The consequent
432 essentiality would further explain why the double deletion of *nuo* and *ndh2* was lethal.
433 The observation shows that ΔΔ*ndh* is only growth impaired in the mid- to late-
434 exponential phase. This indicates that either the Nuo complex is less active in the late
435 growth phase or that the PQQ-dependent glucose dehydrogenase activity during the
436 early growth phase enables sufficient ATP synthesis independent of NADH
437 dehydrogenase activity.

438

439 **Table 4.** Specific NADH oxidation activities of inverted membrane vesicles of *P.*
440 *taiwanensis* VLB120 wild type and NADH dehydrogenase mutants at early and late-
441 exponential growth phase.

Strain	**Specific NADH oxidation activity[a] (U $mg_{protein}^{-1}$)**	
	Early-exponential	**Late-exponential**
Wild type	1.2 ± 0.2	0.7 ± 0.2
Δ*ndh1*	1.3 ± 0.1	0.5 ± 0.1
Δ*ndh2*	1.0 ± 0.2	0.4 ± 0.1
ΔΔ*ndh*	1.1 ± 0.1	0.5 ± 0.2
Δ*nuo*	1.2 ± 0.1	0.5 ± 0.1
Δ*nuo*Δ*ndh1*	0.8 ± 0.1	0.5 ± 0.2

[a] Mean values and standard deviations were determined from independent, biological triplicates

442

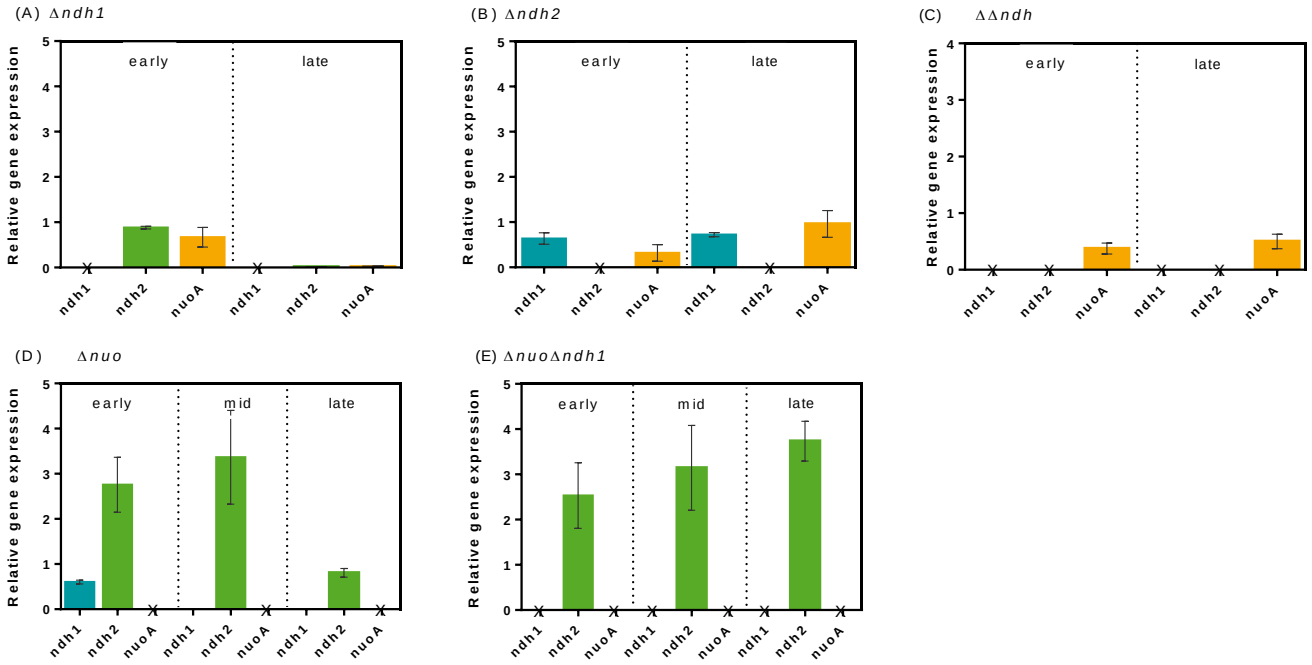

Figure 3. Relative gene expression of the NADH dehydrogenase encoding genes *ndh1*, *ndh2*, and *nuoA* in NADH dehydrogenase mutants Δ*ndh1* (A), Δ*ndh2* (B), ΔΔ*ndh* (C), Δ*nuo* (D), and Δ*nuo*Δ*ndh1* (E) at early-, mid-, and late-exponential growth phase normalized to the corresponding values of the wild type. mRNA abundance was determined by quantitative PCR. Values were normalized to the relative transcript level of *P. taiwanensis* VLB120 in the corresponding growth phase. *nuoA* was used as a proxy for the expression of the *nuo* operon. Gene deletions in the respective mutant are marked with 'X' and were not analyzed by qPCR. Experiments were performed in biological triplicates.

Double deletion of the type II NADH dehydrogenases affect intracellular redox cofactor levels

We found that the NADH oxidation rate was not or only slightly compromised by the introduced gene deletions but that the *ndh2* level was significantly upregulated suggesting that its expression is controlled by the NADH level. For that reason, we determined the intracellular abundance of NADH and NAD^+ in the early-, mid-, and late-exponential growth phase. Since the two single mutants of type II had no growth

phenotype and showed no obvious changes on the transcriptional level, we restricted the analysis to the two double mutants and single *nuo* deletion mutant Δ*nuo*, ΔΔ*ndh,* and Δ*nuo*Δ*ndh1*.

The Δ*nuo*Δ*ndh1* showed a higher NADH/NAD$^+$ ratio in the late-exponential growth phase but also high variability in the triplicate experiments curtailing the statistical significance. The double mutant ΔΔ*ndh* had a significantly increased NADH/NAD$^+$ ratio in the mid- and late-exponential growth phase compared to the wild type (Figure 4). This significantly increased NADH/NAD$^+$ ratio in ΔΔ*ndh* might have triggered the observed growth change in the mid-exponential growth phase.

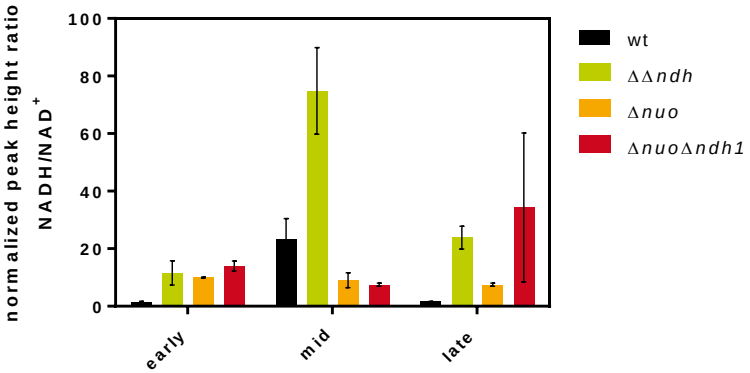

Figure 4. Quantification of the NADH/NAD$^+$ ratio in the *P. taiwanensis* VLB120 and the NADH dehydrogenase mutants ΔΔ*ndh*, Δ*nuo*, and Δ*nuo*Δ*ndh1* in early-, mid- and late-exponential growth phase.

Proteomic analysis reveals rerouting of the carbon flux in the ΔΔ*ndh* mutant

We further performed shotgun proteomic analysis to explain possible metabolic changes in early-, mid-, and late-exponential growth phase in *P. taiwanensis* VLB120 due to NADH dehydrogenase deletions. The relative quantitative results were used to categorize the detected proteins into three groups: (1) Significantly upregulated or (2) downregulated proteins (fold change > 2, adjusted p-value < 0.05), and (3) weak/no effect proteins (fold change < 2). The proteins were further grouped into functional categories according to the KEGG database classification (46), e.g., transport,

carbohydrate metabolism, amino acid metabolism, Supplementary Table S 2) the most strongly represented categories are summarized in Figure 5.

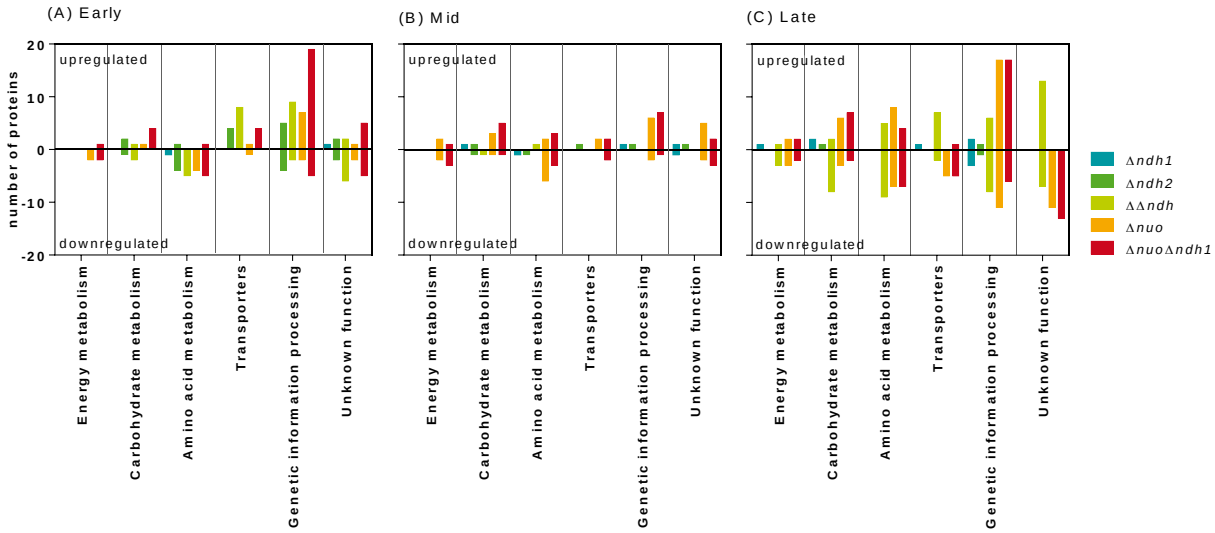

Figure 5. Significant changes at proteome level of *P. taiwanensis* VLB120 NADH dehydrogenase mutants in early- (A), mid- (B), and late-exponential (C) growth phase relative to the wild type. Proteins are clustered into functional categories according to the KEGG classification system (46). Each bar represents the number of proteins in the depicted category the abundance of which was either increased or decreased in response to NADH dehydrogenase deficiency. Experiments were performed in biological triplicates.

In accordance with the physiological and transcript data, we did not observe major changes in the proteome for either NADH dehydrogenase type II single mutants (Δ*ndh1*: 9 of 24 proteins significantly up/downregulated, Δ*ndh2*: 8 of 36 proteins significantly up-/downregulated; Figure 5, Supplementary Table S2, Supplementary File S3). Proteomic changes in both type I mutants (Δ*nuo*: 50 of 139 proteins significantly up-/downregulated, Δ*nuo*Δ*ndh1*: 60 of 165 proteins significantly up-/downregulated) were more significant compared to the type II single gene knockout mutants and very similar to each other (Figure 5). The double deletion mutant ΔΔ*ndh* showed more alterations in

the proteome in the early- and late-exponential phase (17 and 37 of 107 proteins significantly up-/downregulated) than in the mid-exponential phase (2 significantly up-/downregulated proteins) (Figure 5 and Supplementary Table S2).

In the following paragraphs we are focusing on changes observed the ΔΔ*ndh* mutant for proteins related to carbon uptake, energy generation, and oxidative stress response and highlight particular differences to the type 1 NADH dehydrogenase mutants.

The OprB-I porin (PVLB_20075), a carbohydrate selective porin, and the D-gluconate transporter GntT (PVLB_13665) located in the outer and inner membrane, respectively, were higher increased in the ΔΔ*ndh* mutant during the early- and late-exponential growth phase, while the glucokinase quantity was strongly reduced in all growth phases. These data suggest that ΔΔ*ndh* oxidized glucose via glucose dehydrogenase (Gcd) to gluconate to a greater extent than the wild type. In contrast, the quantity of OprB-I in the type I NADH dehydrogenase mutants during the later growth phase was decreased. This might, however, be explained by the faster glucose depletion in these mutants (Figure 1).

During the late-exponential growth of the ΔΔ*ndh* mutant, all enzymes of the arginine deiminase (ADI) pathway were more strongly expressed while they were significantly downregulated in the NADH dehydrogenase type I mutants (Table 6). This pathway catalyzes a three-step conversion of arginine to ornithine, ammonium, and carbon dioxide coupled to ATP generation (47). Likewise, the isocitrate lyase (AceA), the first enzyme of the glyoxylate shunt, was upregulated in the ΔΔ*ndh* mutant but downregulated in the Δ*nuo* mutant, which rather showed a slight upregulation of the 2-oxoglutarate dehydrogenase complex of the TCA cycle during mid- and late-exponential growth. These changes indicate that the mutant ΔΔ*ndh* used the glyoxylate shunt and not exclusively the TCA cycle in the late-exponential growth phase.

We further observed remarkable changes of proteins combating oxidative stress. While deletion of the *nuo* operon (Δ*nuo* and Δ*nuo*Δ*ndh1)* resulted in a generally reduced

529 abundance of proteins involved in the oxidative stress response, those mutants deficient
530 in one of the two type II dehydrogenases displayed increased levels of peroxidases and
531 peroxiredoxin proteins. The abundance of the catalase-peroxidase KatG was extremely
532 decreased in both type I mutants whereas it was weakly increased in the ΔΔ*ndh* mutant.
533 Additionally, the peroxidase encoded by PP_0235 and the quinone reductase ChrR
534 were only higher expressed in the ΔΔ*ndh* mutant with the latter being reported to be
535 induced by superoxide (48) while peroxiredoxin AhpC was weakly upregulated in the
536 single gene deletion mutants, Δ*ndh1* and Δ*ndh2* (Supplementary File S3). These
537 findings indicate that the deletion of the *nuo* complex reduces oxidative stress while it is
538 increased in the mutants deficient in type I dehydrogenase.
539

Table 5. Protein abundance in NADH dehydrogenase mutants in comparison to the wild type. Proteins marked with a diamond (◊) are discussed in the text.

			ΔΔ*ndh*			Δ*nuo*			Δ*nuo*Δ*ndh1*		
			early	mid	late	early	mid	late	early	mid	Late
	Gene name	**Gene function or product**[a]	**Log2 fold change relative to the wild type**[b]								
	Carbohydrate metabolism										
	Pgk	Phosphoglycerate kinase									
	SucC	Succinate-CoA ligase, subunit beta				0.3	0.3	0.5	0.4	0.4	0.5
	SucD	Succinate-CoA ligase, subunit alpha					0.4	1.0	0.6	0.8	1.0
	SdhB	Succinate dehydrogenase						0.8	0.5	0.5	0.8
◊	Glk	Glucokinase	-3.1	-2.8	-2.5						
	TktA	Transketolase			-1.5						
◊	AceA	Isocitrate lyase			0.8			-1.3			
	Ppc	Phosphoenolpyruvate carboxylase					1.35				
	Idh	Isocitrate dehydrogenase						0.6		0.5	-2.6
◊	Gcd	Quinoprotein glucose dehydrogenase						2.2			
	Energy metabolism										
	TsaA	Putative peroxiredoxin					0.5	0.7	0.5	0.48	0.79
	Fpr-I	Ferredoxin-NADP(+) reductase	-1.0		-1.1				-3.1	-1.7	
◊	PP_0235	Peroxidase			3.2						
◊	ChrR	Quinone reductase			2.0						
	Amino acid metabolism										
◊	ArcA	Arginine deiminase			1.1			-1.9			-1.9
◊	ArcB	Ornithine carbamoyltransferase			1.2			-2.3			-2.3
◊	ArcC	Carbamate kinase			0.8	-0.6		-2.0			-1.5
	Transporter/Carbon uptake										
◊	OprB-I	Porin	1.4		1.4			-2.5		-2.0	-2.8
◊	GntT	D-gluconate transporter	0.6		1.2				0.9		
	GtsA	Mannose/glucose ABC transporter	0.8			0.9	0.8		1.0	0.7	
	GtsD	Mannose/glucose ABC transporter	0.7								
	Stress proteins										
◊	KatG	Catalase-peroxidase			0.7			-2.3			-2.8
	TauA	Taurine ABC transporter			2.4						
	DnaK	Chaperone protein			-0.3						
	TrxA	Thioredoxin	0.9		0.6						

Color key

-3	-2	-1		1	2	3

Fold change

[a] Gene function assignment differs from Figure 5

[b] Numbers indicate fold change for upregulated (+) and down regulated (-) proteins relative to the wild type, and the lack of a number indicates no differential production.

Discussion

The presented in-depth analysis of NADH dehydrogenase mutants revealed a high metabolic robustness of *P. taiwanensis* VLB120 to partial loss of the three NADH dehydrogenases, but also the essentiality of residual NADH dehydrogenase activity, as the simultaneous deficiency of Nuo and Ndh2 was lethal likely due to inefficient NADH oxidation or ATP provision.

In accordance with the observed phenotypic robustness, NADH oxidation activities in the mutant strains were not reduced. While this can be explained for those mutants deficient in the *nuo* operon with a significant upregulation of *ndh2*, no transcriptional changes of NADH dehydrogenase related genes were observed for the other mutants. In contrast the mutant with Nuo as the sole NADH dehydrogenase (ΔΔ*ndh*) showed a growth phenotype upon mid-exponential growth phase, accompanied by various metabolic changes summarized in Figure 6. The wild type like growth of the ΔΔ*ndh* mutant on glucose is likely sustained by switching from glucose phosphorylation to direct oxidation in order to partially uncouple the oxidation of the carbon source from NADH formation.

In vitro studies have shown the formation of reactive oxygen species (ROS) such as superoxide ($O_2^{\bullet-}$) and hydrogen peroxide (H_2O_2) by enzymes of the electron transport chain due to electron leakage to oxygen. Nuo (complex I) and cytochrome bc1 (complex III) are considered the main sites for ROS in mitochondria and *P. fluorescens* (49, 50) but rather the type 2 dehydrogenase in, e.g., *E. coli* (51). It has further been reported that an oversupply of NADH can enhance ROS production (52, 53), which activates the cellular antioxidant defense system and can lead to cell death (49, 54). Due to a relatively high $NADH/NAD^+$ ratio in the mid-exponential growth phase, ΔΔ*ndh* might have been faced with higher ROS production than the wild type. This hypothesis is

572 supported by the RAMOS data (Figure 2), which indicated product inhibition after six
573 hours potentially caused by high NADH levels or oxidative stress. In line with this
574 hypothesis, it has been shown that *M. tuberculosis* NADH dehydrogenase mutants with
575 a similarly elevated NADH/NAD^+ ratio were more susceptible to (additional) oxidative
576 stress than those with a lower NADH/NAD^+ ratio (55). Increased ROS production due to
577 an increased NADH/NAD^+ ratio could be one reason for the strongly reduced growth
578 rate in the later growth stages and the trigger for metabolic rerouting in ΔΔ*ndh* (Figure
579 6).
580 The activation of the glyoxylate shunt as indicated by the proteome data might further
581 contribute to stress reduction in two ways. Firstly, this shortcut of the TCA cycle
582 bypasses NADH-producing steps, effectively attenuating NADH generation (56-58).
583 Secondly, the glyoxylate formed by the isocitrate lyase AceA activity of this pathway,
584 upregulated in ΔΔ*ndh*, might react with hydrogen peroxide to produce formate and CO_2
585 (56, 59). This ROS combating strategy was also reported in *Pseudomonas aeruginosa*,
586 *Burkholderia cenocepacia*, and *Staphylococcus aureus*, even though *S. aureus* has no
587 functional glyoxylate shunt (56, 60-62). Note, however, that neither higher formate
588 dehydrogenase abundance nor formate accumulation was observed.
589 ROS production seems to be not elevated in the *nuo* mutants with supposedly higher
590 Ndh2 activity because our data showed no activation of any of these mechanisms. The
591 same was suggested for corresponding *M. tuberculosis* mutants (55).
592 A probable energy shortage due to reduced respiratory activity might have been
593 counteracted in ΔΔ*ndh* by activation of the ADI pathway as an alternative ATP source.
594 This pathway generates 1 mol ATP per mol arginine (47, 63) and was described in *P.*
595 *aeruginosa* to provide ATP under oxygen limiting conditions (47). We exclude oxygen
596 limitation as an inducer of the ADI pathway in *P. taiwanensis* VLB120 under the
597 conditions tested here since the pathway was only expressed in the ΔΔ*ndh* mutant,
598 although all analyzed strains were grown under the same conditions and had similar

oxygen uptake rates. Rather, energy depletion might have activated the ADI pathway in ΔΔ*ndh* on gluconate as described in lactic bacteria (64) or other *Pseudomonas* strains (65), e.g., in *P. putida* DOT-T1E under energy-demanding solvent stress conditions (66, 67).

In this study, we showed a high metabolic flexibility of *P. taiwanensis* VLB120 to interventions in the redox metabolism, which confers robust phenotypic behavior by rerouting of metabolic fluxes. This metabolic adaptability and phenotypic robustness can be advantageous for biocatalysis but simultaneously be challenging because it impedes the prediction of mutant behavior and can lever out metabolic engineering efforts. Hence, to effectively turn this promising microbe into a controllable, biotechnological workhorse, further systems biological and physiological analyses are needed.

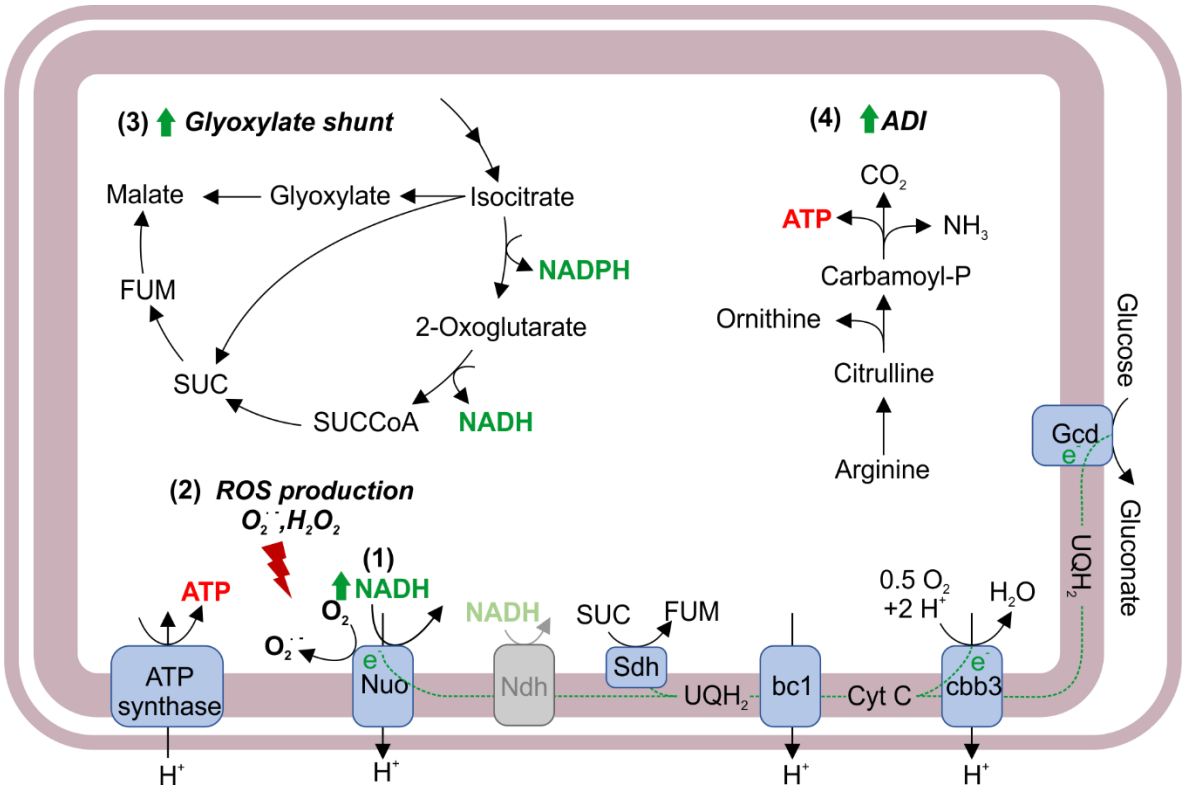

Figure 6. Putative rerouting of the carbon flux caused by type II NADH dehydrogenase deficiency in *P. taiwanensis* VLB120. An increased NADH/NAD$^+$ ratio ***(1)*** triggers ROS production ***(2)*** by NADH dehydrogenase Nuo activity (52, 53). The corresponding cell response to oxidative stress is rerouting the carbon flux through the TCA cycle into the glyoxylate shunt ***(3)*** to reduce NADH formation (56-58) and scavenging of reactive oxygen species by glyoxylate (56, 59). Limited ATP provision from oxidative

phosphorylation might be mitigated by upregulation of the ADI pathway **(*4*)** (65, 66). The light representation of the Ndh dehydrogenase indicates deficiency of both isozymes. ETC, electron transport chain; ROS, reactive oxygen species; ADI, arginine deiminase pathway; Nuo, type I NADH dehydrogenase; Ndh, type II NADH dehydrogenase; Sdh, succinate dehydrogenase; bc1, cytochrome bc1 (complex III); cbb3, cytochrome cbb3 (complex IV); QH_2, ubiquinol; Q, ubiquinone; SUC, succinate, SUCCoA, succinyl-CoA; FUM, fumarate.

Acknowledgement

This study has been conducted within the ERA SynBio project SynPath (Grant ID 031A459) with financial support of the German Federal Ministry of Education and Research and is part of the Joint BioEnergy Institute, supported by the Office of Science, Office of Basic Energy Sciences and Office of Biological and Environmental Research of the U.S. Department of Energy under Contract No. DE-AC02-05CH11231. BEE and SCN acknowledge financial support by the German Academic Exchange Service (DAAD) through the thematic network Aachen-California Network of Academic Exchange (ACalNet) funded by the German Federal Ministry of Education and Research (BMBF). LMB acknowledges funding by the Cluster of Excellence "The Fuel Science Center - Adaptive Conversion Systems for Renewable Energy and Carbon Sources" (EXC 2186), which is funded by the Excellence Initiative of the German federal and state governments to promote science and research at German universities. We thank Stephani Baum and Uwe Conrath for sharing lab equipment and for technical support. We are grateful to Itay Budin for discussions and instruction on the membrane isolation and *in vitro* assays and Sophia Nölting for support with qPCR measurements. We thank Benedikt Wynands and Nick Wierckx for sharing the strain *P. taiwanensis* VLB120 $pSTY^-$ and Victor de Lorenzo (Centro Nacional de Biotechnología - CNB, Madrid) for providing plasmid pEMG.

References

1. Kracke F, Kromer JO. 2014. Identifying target processes for microbial electrosynthesis by elementary mode analysis. BMC Bioinformatics 15:410.
2. Köhler KA, Blank LM, Frick O, Schmid A. 2015. D-Xylose assimilation via the Weimberg pathway by solvent-tolerant *Pseudomonas taiwanensis* VLB120. Environ Microbiol 17:156-170.
3. Becker J, Lange A, Fabarius J, Wittmann C. 2015. Top value platform chemicals: bio-based production of organic acids. Curr Opin Biotechnol 36:168-175.
4. Yim H, Haselbeck R, Niu W, Pujol-Baxley C, Burgard A, Boldt J, Khandurina J, Trawick JD, Osterhout RE, Stephen R, Estadilla J, Teisan S, Schreyer HB, Andrae S, Yang TH, Lee SY, Burk MJ, Van Dien S. 2011. Metabolic engineering of *Escherichia coli* for direct production of 1,4-butanediol. Nat Chem Biol 7:445.
5. Nakamura CE, Whited GM. 2003. Metabolic engineering for the microbial production of 1,3-propanediol. Curr Opin Biotechnol 14:454-459.
6. Takeno S, Murata R, Kobayashi R, Mitsuhashi S, Ikeda M. 2010. Engineering of *Corynebacterium glutamicum* with an NADPH-generating glycolytic pathway for L-lysine production. Appl Environ Microbiol 76:7154-7160.
7. Fasan R, Crook NC, Peters MW, Meinhold P, Buelter T, Landwehr M, Cirino PC, Arnold FH. 2011. Improved product-per-glucose yields in P450-dependent propane biotransformations using engineered *Escherichia coli*. Biotechnol Bioeng 108:500-510.
8. Becker J, Zelder O, Hafner S, Schroder H, Wittmann C. 2011. From zero to hero-design-based systems metabolic engineering of *Corynebacterium glutamicum* for L-lysine production. Metab Eng 13:159-168.
9. Berríos-Rivera SJ, Bennett GN, San K-Y. 2002. Metabolic Engineering of *Escherichia coli*: increase of NADH availability by overexpressing an NAD^+-dependent formate dehydrogenase. Metab Eng 4:217-229.
10. Jain R, Huang J, Yuan Q, Yan Y. 2015. Engineering microaerobic metabolism of *E. coli* for 1,2-propanediol production. J Ind Microbiol Biotechnol 42:1049-1055.
11. Blank LM, Ebert BE, Buhler B, Schmid A. 2008. Metabolic capacity estimation of *Escherichia coli* as a platform for redox biocatalysis: constraint-based modeling and experimental verification. Biotechnol Bioeng 100:1050-1065.
12. Blank LM, Ionidis G, Ebert BE, Bühler B, Schmid A. 2008. Metabolic response of *Pseudomonas putida* during redox biocatalysis in the presence of a second octanol phase. FEBS J 275:5173-5190.
13. Julsing MK, Kuhn D, Schmid A, Bühler B. 2012. Resting cells of recombinant *E. coli* show high epoxidation yields on energy source and high sensitivity to product inhibition. Biotechnol Bioeng 109:1109-1119.
14. Ebert BE, Kurth F, Grund M, Blank LM, Schmid A. 2011. Response of *Pseudomonas putida* KT2440 to increased NADH and ATP demand. Appl Environ Microbiol 77:6597-6605.
15. Rühl J, Schmid A, Blank LM. 2009. Selected *Pseudomonas putida* strains able to grow in the presence of high butanol concentrations. Appl Environ Microbiol 75:4653-4656.
16. Wynands B, Lenzen C, Otto M, Koch F, Blank LM, Wierckx N. 2018. Metabolic engineering of *Pseudomonas taiwanensis* VLB120 with minimal genomic modifications for high-yield phenol production. Metab Eng 47:121-133.
17. Wierckx NJP, Ballerstedt H, Bont JaMD, Wery J. 2005. Engineering of solvent-tolerant *Pseudomonas putida* S12 for bioproduction of phenol from glucose. Appl Environ Microbiol 71:8221-8227.

18. Tiso T, Sabelhaus P, Behrens B, Wittgens A, Rosenau F, Hayen H, Blank LM. 2016. Creating metabolic demand as an engineering strategy in *Pseudomonas putida* – rhamnolipid synthesis as an example. Metab Eng Commun 3:234-244.
19. Dong J, Chen Y, Benites VT, Baidoo EEK, Petzold CJ, Beller HR, Eudes A, Scheller HV, Adams PD, Mukhopadhyay A, Simmons BA, Singer SW. 2019. Methyl ketone production by *Pseudomonas putida* is enhanced by plant-derived amino acids. Biotechnol Bioeng doi:10.1002/bit.26995.
20. Park JB, Buhler B, Panke S, Witholt B, Schmid A. 2007. Carbon metabolism and product inhibition determine the epoxidation efficiency of solvent-tolerant *Pseudomonas sp*. strain VLB120ΔC. Biotechnol Bioeng 98:1219-1229.
21. Foster JW, Park YK, Penfound T, Fenger T, Spector MP. 1990. Regulation of NAD metabolism in *Salmonella typhimurium*: molecular sequence analysis of the bifunctional *nadR* regulator and the *nadA-pnuC* operon. J Bacteriol 172:4187-4196.
22. Spehr V, Schlitt A, Scheide D, Guénebaut V, Friedrich T. 1999. Overexpression of the *Escherichia coli nuo*-operon and isolation of the overproduced NADH:ubiquinone oxidoreductase (complex I). Biochemistry 38:16261-16267.
23. Pruss BM, Nelms JM, Park C, Wolfe AJ. 1994. Mutations in NADH:ubiquinone oxidoreductase of Escherichia coli affect growth on mixed amino acids. J Bacteriol 176:2143-2150.
24. Matsushita K, Ohnishi T, Kaback HR. 1987. NADH-ubiquinone oxidoreductases of the *Escherichia coli* aerobic respiratory chain. Biochemistry 26:7732-7737.
25. Sambrook J, E.F. Fritsch, and T. Maniatis. 1982. Molecular Cloning: a laboratory manual. Cold Spring Harbour Press.
26. Hartmans S, Smits JP, van der Werf MJ, Volkering F, de Bont JA. 1989. Metabolism of styrene oxide and 2-phenylethanol in the styrene-degrading *Xanthobacter* strain 124X. Appl Environ Microbiol 55:2850-2855.
27. Ditta G, Stanfield S, Corbin D, Helinski DR. 1980. Broad host range DNA cloning system for Gram-negative bacteria: construction of a gene bank of *Rhizobium meliloti*. Proc Nat Acad Sci USA 77:7347-7351.
28. Martínez-García E, de Lorenzo V. 2011. Engineering multiple genomic deletions in Gram-negative bacteria: Analysis of the multi-resistant antibiotic profile of *Pseudomonas putida* KT2440. Environ Microbiol 13:2702-2716.
29. Panke S, Witholt B, Schmid A, Wubbolts MG. 1998. Towards a biocatalyst for (*S*)-styrene oxide production: characterization of the styrene degradation pathway of *Pseudomonas* sp. strain VLB120. Appl Environ Microbiol 64:2032-2043.
30. Choi KH, Kumar A, Schweizer HP. 2006. A 10-min method for preparation of highly electrocompetent *Pseudomonas aeruginosa* cells: application for DNA fragment transfer between chromosomes and plasmid transformation. J Microbiol Methods 64:391-397.
31. Chomczynski P, Rymaszewski M. 2006. Alkaline polyethylene glycol-based method for direct PCR from bacteria, eukaryotic tissue samples, and whole blood. BioTechniques 40:454, 456, 458.
32. Gonzalez Fernandez-Nino SM, Smith-Moritz AM, Chan LJ, Adams PD, Heazlewood JL, Petzold CJ. 2015. Standard flow liquid chromatography for shotgun proteomics in bioenergy research. Front Bioeng Biotechnol 3:44.
33. Perez-Riverol Y, Csordas A, Bai J, Bernal-Llinares M, Hewapathirana S, Kundu DJ, Inuganti A, Griss J, Mayer G, Eisenacher M, Perez E, Uszkoreit J, Pfeuffer J, Sachsenberg T, Yilmaz S, Tiwary S, Cox J, Audain E, Walzer M, Jarnuczak AF, Ternent T, Brazma A, Vizcaino JA. 2019. The PRIDE database and related tools and resources in 2019: improving support for quantification data. Nucleic Acids Res 47:D442-D450.

34. Pfaffl MW. 2001. A new mathematical model for relative quantification in real-time RT-PCR. Nucleic Acids Res 29:e45.
35. Borisov VB, Murali R, Verkhovskaya ML, Bloch Da, Han H, Gennis RB, Verkhovsky MI. 2011. Aerobic respiratory chain of *Escherichia coli* is not allowed to work in fully uncoupled mode. Proc Natl Acad Sci U S A 108:17320-17324.
36. Schulte A, Schilling JV, Nolten J, Korona A, Krömke H, Vennekötter J-B, Schillheim B, Wessling M, Conrath U, Büchs J. 2018. Parallel online determination of ethylene release rate by Shaken Parsley cell cultures using a modified RAMOS device. BMC Plant Biol 18:101.
37. Anderlei T, Zang W, Papaspyrou M, Buchs J. 2004. Online respiration activity measurement (OTR, CTR, RQ) in shake flasks. Biochem Eng J 17:187-194.
38. McCloskey D, Utrilla J, Naviaux RK, Palsson BO, Feist AM. 2015. Fast Swinnex filtration (FSF): a fast and robust sampling and extraction method suitable for metabolomics analysis of cultures grown in complex media. Metabolomics 11:198-209.
39. Wu L, Mashego MR, van Dam JC, Proell AM, Vinke JL, Ras C, van Winden WA, van Gulik WM, Heijnen JJ. 2005. Quantitative analysis of the microbial metabolome by isotope dilution mass spectrometry using uniformly ^{13}C-labeled cell extracts as internal standards. Anal Biochem 336:164-171.
40. Mashego MR, Wu L, Van Dam JC, Ras C, Vinke JL, Van Winden WA, Van Gulik WM, Heijnen JJ. 2004. MIRACLE: mass isotopomer ratio analysis of U-^{13}C-labeled extracts. A new method for accurate quantification of changes in concentrations of intracellular metabolites. Biotechnol Bioeng 85:620-628.
41. Torres A, Kasturiarachi N, DuPont M, Cooper VS, Bomberger J, Zemke A. 2019. NADH dehydrogenases in *Pseudomonas aeruginosa* growth and virulence. Front Microbiol 10.
42. Köhler KAK, Rückert C, Schatschneider S, Vorhölter FJ, Szczepanowski R, Blank LM, Niehaus K, Goesmann A, Pühler A, Kalinowski J, Schmid A. 2013. Complete genome sequence of *Pseudomonas* sp. strain VLB120 a solvent tolerant, styrene degrading bacterium, isolated from forest soil. J Biotechnol 168:729-730.
43. Vicente M, Canovas JL. 1973. Glucolysis in *Pseudomonas putida*: physiological role of alternative routes from the analysis of defective mutants. J Bacteriol 116:908-914.
44. del Castillo T, Ramos JL, Rodriguez-Herva JJ, Fuhrer T, Sauer U, Duque E. 2007. Convergent peripheral pathways catalyze initial glucose catabolism in *Pseudomonas putida*: genomic and flux analysis. J Bacteriol 189:5142-5152.
45. Calhoun MW, Gennis RB. 1993. Demonstration of separate genetic loci encoding distinct membrane-bound respiratory NADH dehydrogenases in *Escherichia coli*. J Bacteriol 175:3013-3019.
46. Kanehisa M, Sato Y, Kawashima M, Furumichi M, Tanabe M. 2016. KEGG as a reference resource for gene and protein annotation. Nucleic Acids Res 44:D457-462.
47. Mercenier A, Simon JP, Vander Wauven C, Haas D, Stalon V. 1980. Regulation of enzyme synthesis in the arginine deiminase pathway of *Pseudomonas aeruginosa*. J Bacteriol 144:159-163.
48. Gonzalez CF, Aekerley DF, Lynch SV, Matin A. 2005. ChrR, a soluble quinone reductase of *Pseudomonas putida* that defends against H_2O_2. J Biol Chem 280:22590-22595.
49. Mailloux RJ, Lemire J, Appanna VD. 2011. Metabolic networks to combat oxidative stress in *Pseudomonas fluorescens*. Antonie Van Leeuwenhoek 99:433-442.
50. Imlay JA. 2003. Pathways of oxidative damage. Annu Rev Microbiol 57:395-418.

51. Messner KR, Imlay JA. 1999. The identification of primary sites of superoxide and hydrogen peroxide formation in the aerobic respiratory chain and sulfite reductase complex of *Escherichia coli*. J Biol Chem 274:10119-10128.
52. Murphy MP. 2009. How mitochondria produce reactive oxygen species. Biochem J 417:1-13.
53. Vinogradov AD, Grivennikova VG. 2016. Oxidation of NADH and ROS production by respiratory complex I. Biochim Biophys Acta 1857:863-871.
54. Sharma LK, Lu J, Bai Y. 2009. Mitochondrial respiratory complex I: structure, function and implication in human diseases. Curr Med Chem 16:1266-1277.
55. Vilcheze C, Weinrick B, Leung LW, Jacobs WR, Jr. 2018. Plasticity of *Mycobacterium tuberculosis* NADH dehydrogenases and their role in virulence. Proc Natl Acad Sci U S A 115:1599-1604.
56. Ahn S, Jung J, Jang IA, Madsen EL, Park W. 2016. Role of glyoxylate shunt in oxidative stress response. J Biol Chem 291:11928-11938.
57. Kornberg HL. 1966. The role and control of the glyoxylate cycle in *Escherichia coli*. The Biochemical journal 99:1-11.
58. Lemire J, Alhasawi A, Appanna VP, Tharmalingam S, Appanna VD. 2017. Metabolic defence against oxidative stress: the road less travelled so far. J Appl Microbiol 123:798-809.
59. Thomas SC, Alhasawi A, Auger C, Omri A, Appanna VD. 2016. The role of formate in combatting oxidative stress. Antonie Van Leeuwenhoek 109:263-271.
60. Van Acker H, Sass A, Bazzini S, De Roy K, Udine C, Messiaen T, Riccardi G, Boon N, Nelis HJ, Mahenthiralingam E, Coenye T. 2013. Biofilm-grown *Burkholderia cepacia* complex cells survive antibiotic treatment by avoiding production of reactive oxygen species. PLoS One 8:e58943.
61. Somerville GA, Proctor RA. 2009. At the crossroads of bacterial metabolism and virulence factor synthesis in *Staphylococci*. Microbiol Mol Biol Rev 73:233-248.
62. Somerville GA, Said-Salim B, Wickman JM, Raffel SJ, Kreiswirth BN, Musser JM. 2003. Correlation of acetate catabolism and growth yield in *Staphylococcus aureus*: implications for host-pathogen interactions. Infect Immun 71:4724-4732.
63. Thauer RK, Jungermann K, Decker K. 1977. Energy conservation in chemotrophic anaerobic bacteria. Bacteriol Rev 41:100-180.
64. Fernández M, Zúñiga M. 2006. Amino acid catabolic pathways of lactic acid bacteria. Crit Rev Microbiol 32:155-183.
65. Cunin R, Glansdorff N, Piérard A, Stalon V. 1986. Biosynthesis and metabolism of arginine in bacteria. Microbiol Rev 50:314-352.
66. Segura A, Godoy, P., van Dillewijn, P., Hurtado, A., Arroyo, N., Santacruz, S., Ramos, J.-L. 2005. Proteomic analysis reveals the participation of energy- and stress-related proteins in the response of *Pseudomonas putida* DOT-T1E to toluene J Bacteriol 187:5937-5945.
67. Ramos JL, Duque E, Rodriguez-Herva JJ, Godoy P, Haidour A, Reyes F, Fernandez-Barrero A. 1997. Mechanisms for solvent tolerance in bacteria. J Biol Chem 272:3887-3890.

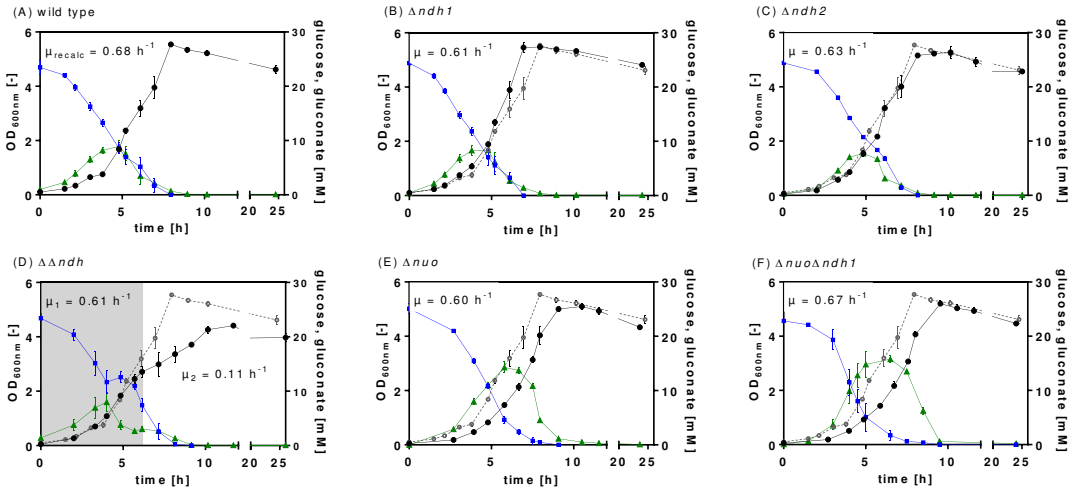
(A) wild type
μrecalc = 0.68 h-1
(B) Δndh1
μ = 0.61 h-1
(C) Δndh2
μ = 0.63 h-1
(D) ΔΔndh
μ1 = 0.61 h-1
μ2 = 0.11 h-1
(E) Δnuo
μ = 0.60 h-1
(F) ΔnuoΔndh1
μ = 0.67 h-1
OD600nm [-]
glucose, gluconate [mM]
time [h]

Figure 1

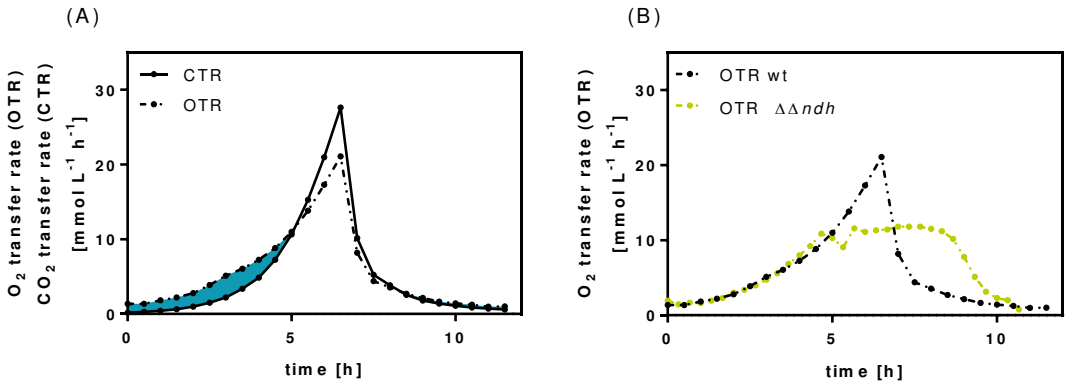
(A)
CTR
OTR
O_2 transfer rate (OTR)
CO_2 transfer rate (CTR)
[mmol L^{-1} h^{-1}]
0
10
20
30
0
5
10
time [h]
(B)
OTR wt
OTR ΔΔ*ndh*
O_2 transfer rate (OTR)
[mmol L^{-1} h^{-1}]
0
10
20
30
0
5
10
time [h]

Figure 2.

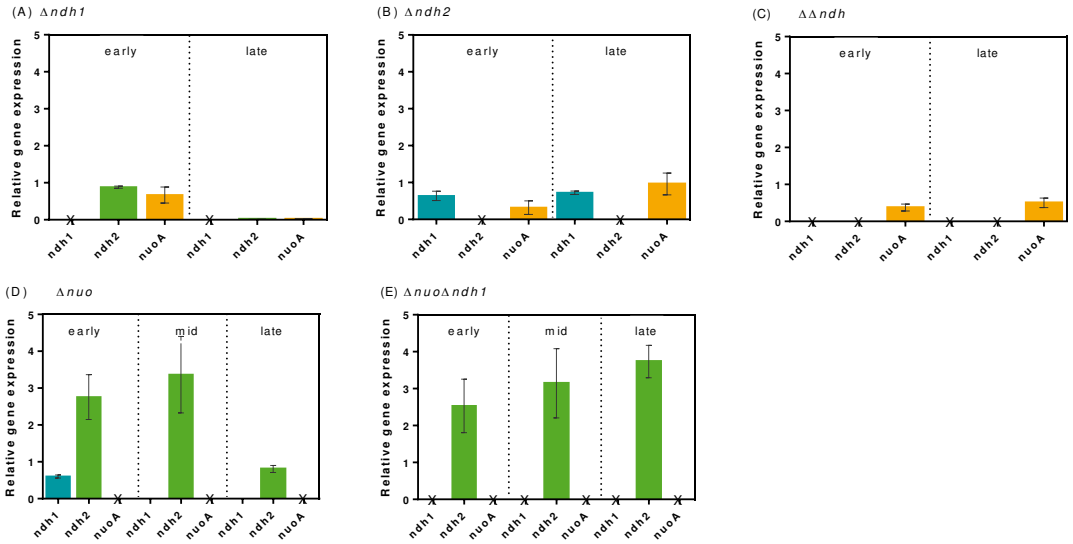
(A) Δndh1
(B) Δndh2
(C) ΔΔndh
(D) Δnuo
(E) ΔnuoΔndh1
Relative gene expression
early
mid
late
ndh1
ndh2
nuoA

Figure 3.

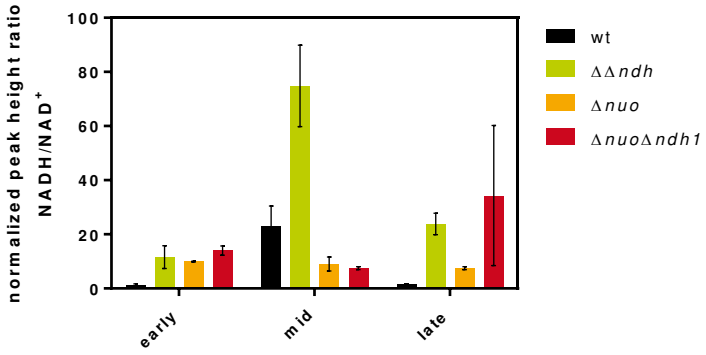
normalized peak height ratio
NADH/NAD+
100
80
60
40
20
0
early
mid
late
wt
ΔΔndh
Δnuo
ΔnuoΔndh1

Figure 4.

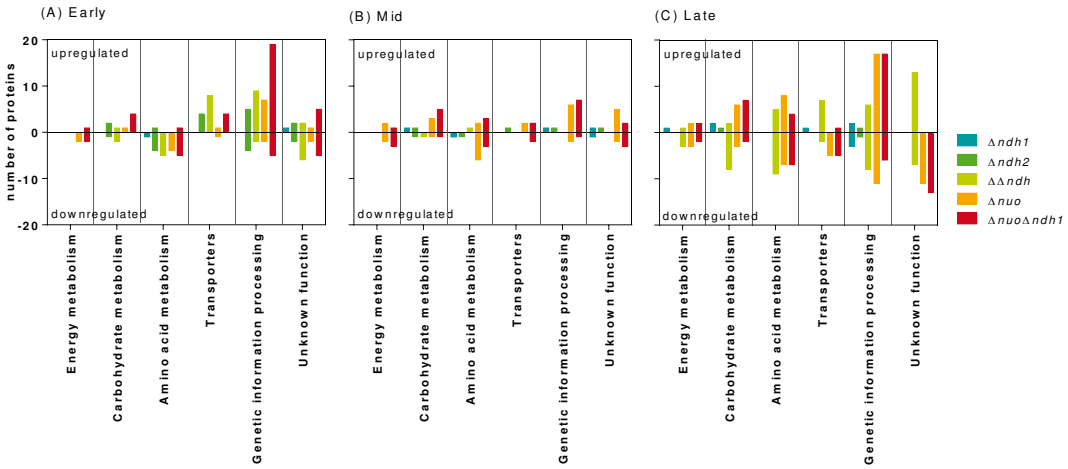
(A) Early
(B) Mid
(C) Late
number of proteins
20
10
0
-10
-20
upregulated
downregulated
Energy metabolism
Carbohydrate metabolism
Amino acid metabolism
Transporters
Genetic information processing
Unknown function
Δndh1
Δndh2
ΔΔndh
Δnuo
ΔnuoΔndh1

Figure 5.

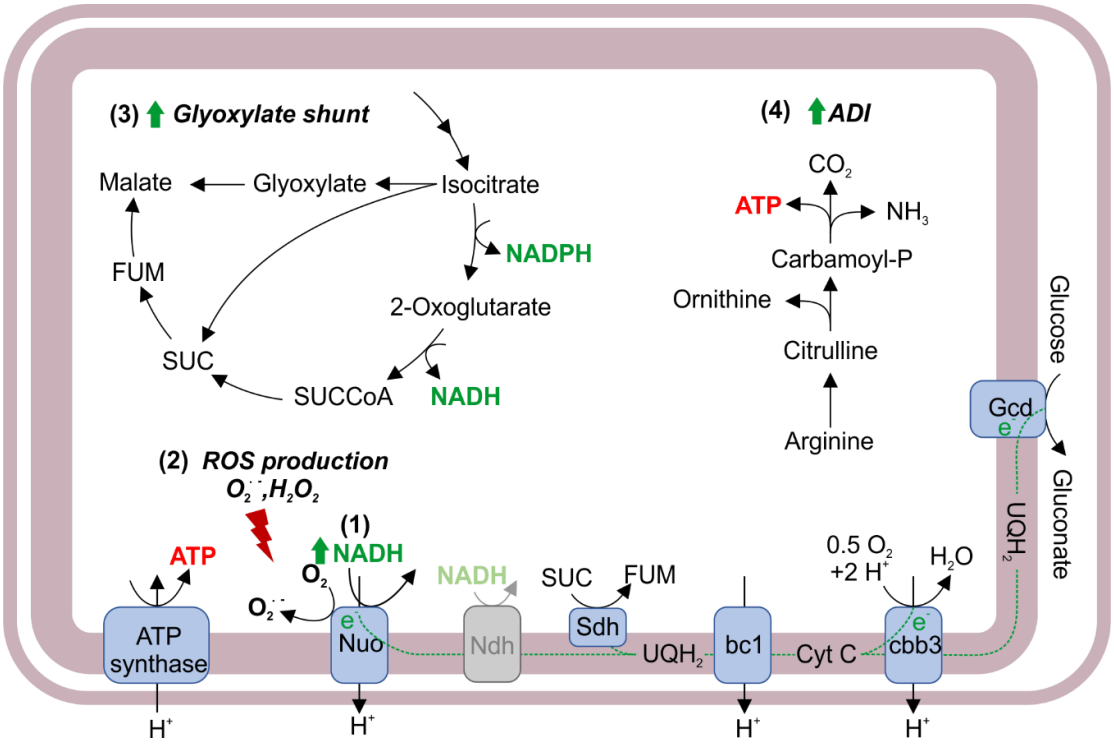
(3) Glyoxylate shunt
Malate
Glyoxylate
Isocitrate
NADPH
FUM
2-Oxoglutarate
SUC
SUCCoA
NADH
(4) ADI
CO2
ATP
NH3
Carbamoyl-P
Ornithine
Citrulline
Arginine
Glucose
Gcd
e
Gluconate
UQH2
(2) ROS production
O2·-,H2O2
(1)
NADH
ATP
O2
O2·-
NADH
SUC
FUM
0.5 O2
+2 H+
H2O
e
ATP synthase
Nuo
Ndh
Sdh
UQH2
bc1
Cyt C
cbb3
H+
H+
H+
H+

Figure 6.